Journal of Electronic Materials (2023) 52:2895–2903
https://doi.org/10.1007/s11664-023-10281-5

TOPICAL COLLECTION: SYNTHESIS AND ADVANCED CHARACTERIZATION OF MAGNETIC OXIDES

Iron-Doped Titania for Magneto-Opto-Electronic Device Applications

Divya Rehani[1,2] · Manish Saxena[3] · Sanjay R. Dhakate[2] · Shailesh Narain Sharma[2]

Received: 29 March 2022 / Accepted: 27 January 2023 / Published online: 21 February 2023

Abstract

Almost a decade ago, transition metal-doped wide-bandgap metal oxides showed a significant contribution to device applications. In combination, they are a promising candidate for applications in electro-magneto-optic devices. In the present study, Fe_2O_3 (hematite ore) (0–5 wt.%)-doped titania (TiO_2) was synthesized by high-temperature solid-state reaction. An increase in secondary phases was observed with high Fe percentage. Further degradation of crystallinity was observed in the x-ray diffraction (XRD) study. The average crystallite size, according to the Williamson–Hall plot, is 42 nm. Vibrating-sample magnetometer (VSM) investigation depicts maximum magnetization for 2% Fe:TiO_2 of 6.2×10^{-1} emu/gm. The absorption spectra showed a higher wavelength shift with the increase in Fe. Similarly, the luminescence spectra underwent quenching with high Fe_2O_3 in the TiO_2. The scanning electron microscopy (SEM) analysis showed all particles with a size of ~ 50 nm. According to the dielectric results, the electrical conductivity of un-doped and low-Fe-doped TiO_2 is weak, whereas it improves at a higher frequency. This study revealed that the 2% Fe:TiO_2 sample shows high crystallinity, maximum emission intensity, high dielectric constant, and maximum magnetization. Thus, 2% iron-doped titania is efficient for magneto-opto-electronic device applications.

Graphical Abstract

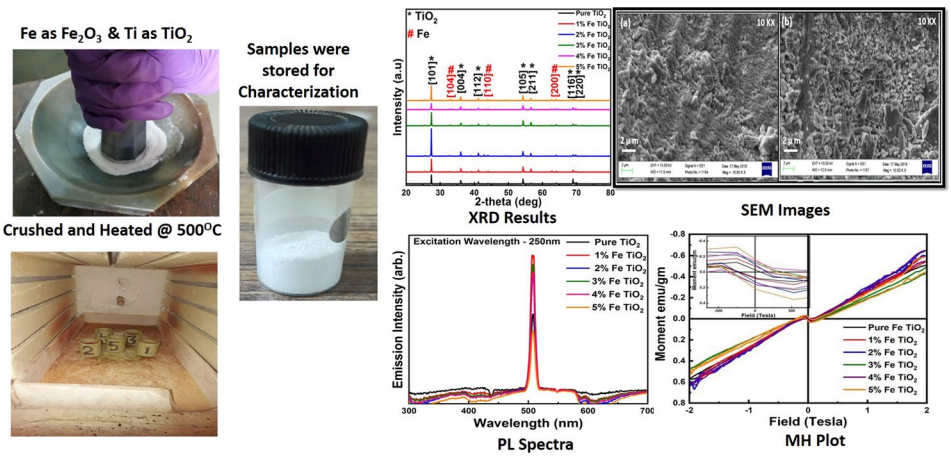

Keywords Titania · crystallographically · magneto-opto-electronic

Introduction

Transition metal-doped semiconductor metal oxides have recently emerged as competitors in numerous applications ranging from optics and electronics to magnetics. Titania

✉ Shailesh Narain Sharma
shailesh@nplindia.org

Extended author information available on the last page of the article

(TiO_2) is most preferred because of its applications as a photo-electrode due to high photo-corrosion resistance in aqueous media, solar cells, optical filtering applications, and strong antimicrobial coatings, etc. Crystallographically, the anatase form of TiO_2 is highly optically active compared with all other phases of titania. Moreover, titania is chemically stable, low-cost, and nontoxic.[1,2] To improve the electrical and magnetic properties of TiO_2, an appropriate percentage of any transition metal oxide can make it effective for magneto-opto-electro applications.[3,4]

Among all the transition metal cations, Fe has attracted special attention because of its three major characteristics: (1) iron takes less charge-carrier recombination time; (2) iron is characterized by a wavelength shift towards a higher range in the spectra of absorption, transmittance, reflectance, or emission range (lower frequency), i.e. redshift; and (3) iron as a dopant enhances the photocatalyst activity because of its great advantages of maximum oxidation and reduction states.[5] All the previously reported synthesis routes are of longer synthesis time for Fe-, Ni-, and Co-doped TiO_2 nanotubes.[6] Other studies have utilized an expensive setup.[7] Fe-doped TiO_2 thin films exhibit room-temperature ferromagnetism, as observed by Rasoulnezhad et al. in 2018.[8] Photoelectrolysis of water into hydrogen and oxygen in photoelectrochemical (PEC) cells was also performed using Fe-doped TiO_2.[2] The addition of magnetic ions in the nonmagnetic matrix system opens up a new perspective in the area of spintronics and magneto-optic device applications.[9] In the present study, we prepare Fe_2O_3 (hematite ore) (0–5% weight percentage)-doped TiO_2 under high-temperature solid-state reaction.

Experiment

Materials and Method

Fe_2O_3 (hematite ore) (0–5% weight percentage)-doped TiO_2 samples were synthesized by a conventional high-temperature solid-state reaction. The Fe_2O_3-doped TiO_2) was weighed and added to a mortar pestle for crushing for about 30 min. All samples were heated at a moderate temperature of 500°C in an air atmosphere. As reported, the TiO_2 sample annealed at 500°C retained a unique anatase phase.[10] Fe_2O_3 doping percentage varied from 0 wt.% to 5 wt.%. Earlier researchers tailored the bandgap of un-doped TiO_2 by varying the doping percentage without affecting the nature of the crystalline structure of anatase TiO_2. An optical energy shift was observed from 3.2 eV to 2.8 eV by the addition of Fe from 0 wt.% to 5 wt.%,[11] whereas the magnetic property improved as doping increased from a lower to a higher percentage.[12] All powders were cooled and crushed for safe storage and further characterization.[13] Many defects occur due to the shifting of atoms, changing the electrical conductivity, optical, and magnetic properties.

The phase investigations were done using a Rigaku Mini-Flex instrument with a Cu-Kα radiation (1.54 Å) source x-ray diffractometer. Scanning electron microscopy (SEM; LEO 440 PC, digital) was employed to visualize all the samples. A UV-3101PC system (Shimadzu) with a broad ultraviolet–visible–near-infrared (UV–VIS–NIR) range of 206–13,825 was harnessed for UV spectra analysis. The photoluminescence (PL) spectrum was recorded by an Edinburgh FLSP920 instrument. The magnetic investigations were performed using a Lake Shore vibrating-sample magnetometer (VSM model no. 7410). UV–Vis spectrophotometer and PL emission studies were performed for optical investigation at an excitation of 250 nm. The electrical conductivity studies were done using a SourceMeter (Keithley-236) and a Hioki LCR meter-3532-50 for current–voltage plots. All studies were done at room temperature for the best possible device applications at room temperature.

Results and Discussion

Structural and Morphological Studies

Results of the x-ray diffraction (XRD) study of synthesized Fe_2O_3 -doped TiO_2 fused at 500°C are plotted in Fig. 1a and b. Peak intensities for all Fe:TiO_2 samples and the crystallite size distribution correspond to the anatase phase of TiO_2. The peaks marked Ti and Fe correspond to anatase TiO_2 and iron, respectively. Diffractions matching well with the anatase phase of TiO_2 crystals (101) are visibly detectable at $2\theta = 25.28°$ as body-centered with tetragonal geometry, where $a = b \sim 3.79$ Å, and $c \sim 9.48$ Å (referenced to file no. 21-1272). Fe_2O_3-doped TiO_2 is shown Fig. 1c. The peaks correspond to the hkl values of (101), (004), (112), (200), (105), (211), (204), (116), (220), and (215) of anatase TiO_2. Secondary growth of Fe is observed with an increase in doping percentage beyond a certain limit, with additional peaks appearing in the XRD spectra; 2% is the optimum doping percentage of Fe in TiO_2. At higher doping percentage, secondary peaks at (211), (220), (110), (321), (200), and (330) resemble the planes of Fe (JCPDS cards 89-4186, 01-1267, and 01-1262). This demonstrate that, initially, there is no change in the basic structure of anatase TiO_2 with the doping of Fe_2O_3. This confirms that Fe^{3+}ions are perfectly fused in the structure of anatase TiO_2 instead of accumulating on TiO_2.

Some additional peaks of Fe can be seen at (211), (220), and (110) after doping of 2% Fe in TiO_2. This signifies secondary growth of Fe overlapping the basic structure of anatase TiO_2. As per the analysis, 2% Fe:TiO_2 has superior

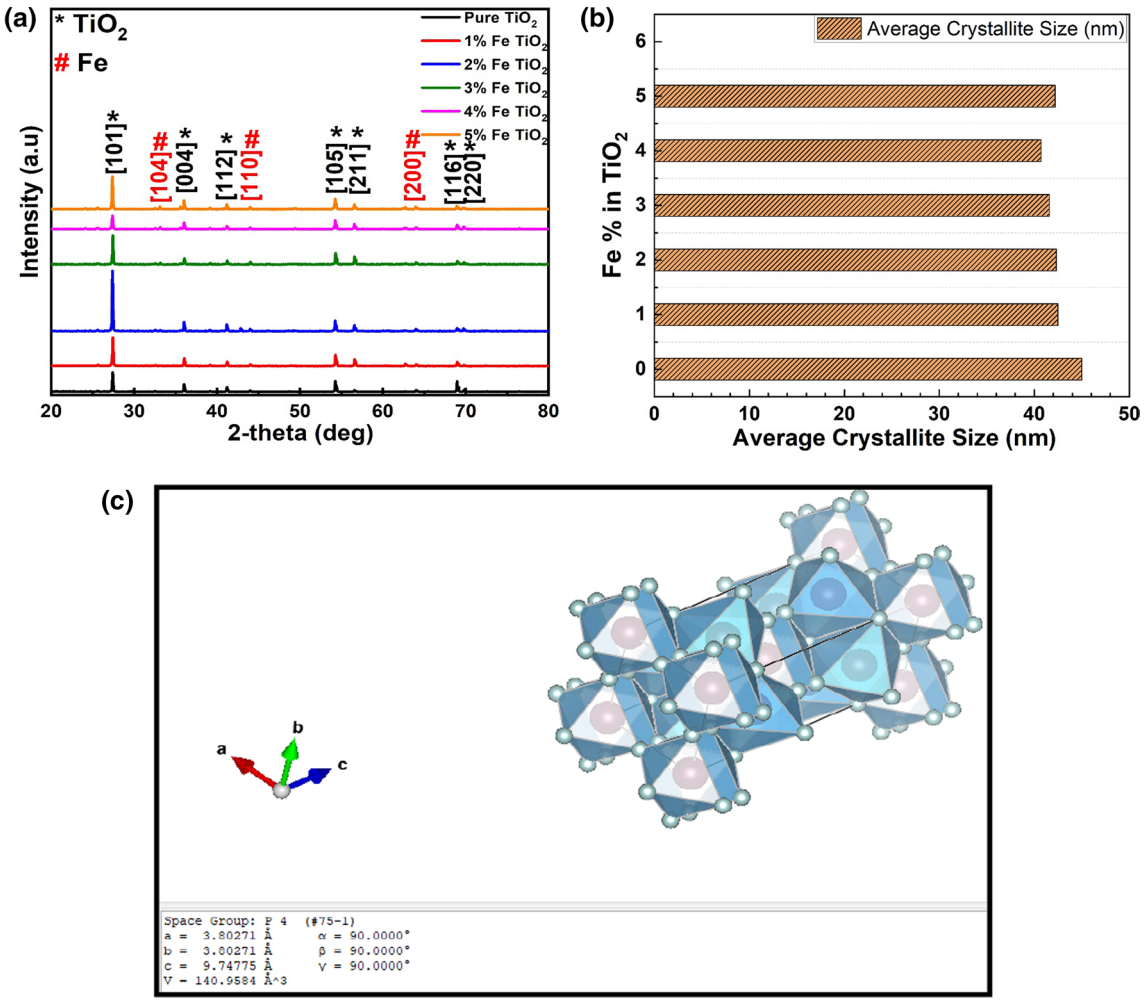

Fig. 1 (a) XRD pattern of un-doped TiO_2 and Fe:TiO_2 samples. (b) Average crystallite size distribution. (c) Crystal structure of tetragonal anatase TiO_2.

crystallinity because at a low doping percentage of Fe, it occupies an interstitial position in TiO_2. Moreover, doping Fe ion into TiO_2 replaces Fe^{3+} with Ti^{4+}which results in the elongation of the metal–anion bond length of the TiO_2 anatase structure.[14]

The Williamson–Hall formulation for crystallite size results as 45 nm, 42.5 nm, 42.3 nm, 41.5 nm, 40.7 nm, and 42.2 nm for un-doped, 1%, 2%, 3%, 4%, and 5% Fe:TiO_2, respectively. The average crystallite size observed was 42 nm. With the addition of Fe in anatase TiO_2, the structure undergoes lattice distortion and reduction in crystallite size. Along with the reduction of crystallite size, Fe also inhibits the transformation of the anatase to a rutile phase, thus resulting in the formation of a metastable anatase phase of Fe:TiO_2.[15]

For structural investigations, an electron gun-equipped microscope was used for un-doped and 2% Fe:TiO_2 samples. Figure 2a and b present SEM images of un-doped TiO_2 and 2% Fe:TiO_2 at magnification 10kx.The SEM images showed the particles are in the range of ~ 50–45 nm for un-doped TiO_2 and 2% Fe:TiO_2. All particles have asymmetrical cluster structures with elongated geometry because of the agglomeration effect. Figure 3a and b shows energy-dispersive x-ray spectroscopy (EDX) for analytical study for un-doped TiO_2 and 2% Fe:TiO_2. The quantitative results showed that Fe is doped in the TiO_2 with approx. 2% by weight.

Magnetic Study: VSM

Magnetism strongly depends upon the experimental technique and the type of transition metal doped in the semiconductor metal oxide. It has been observed that some magnetic impurities add to paramagnetic behavior rather than ferromagnetic behavior in TiO_2.[16] The paramagnetic character remains dominant irrespective of heat treatment given to the samples or during the characterization at 5–1270 K.[17]

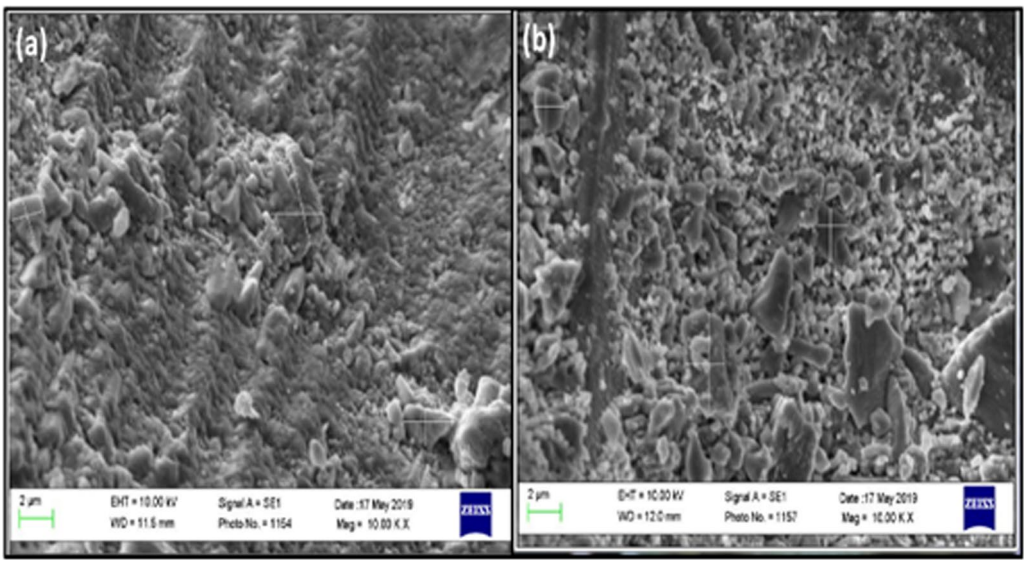

Fig. 2 (a) SEM micrographs of un-doped TiO_2 at magnification 10kx. (b) SEM micrographs of Fe:TiO_2 at magnification 10kx.

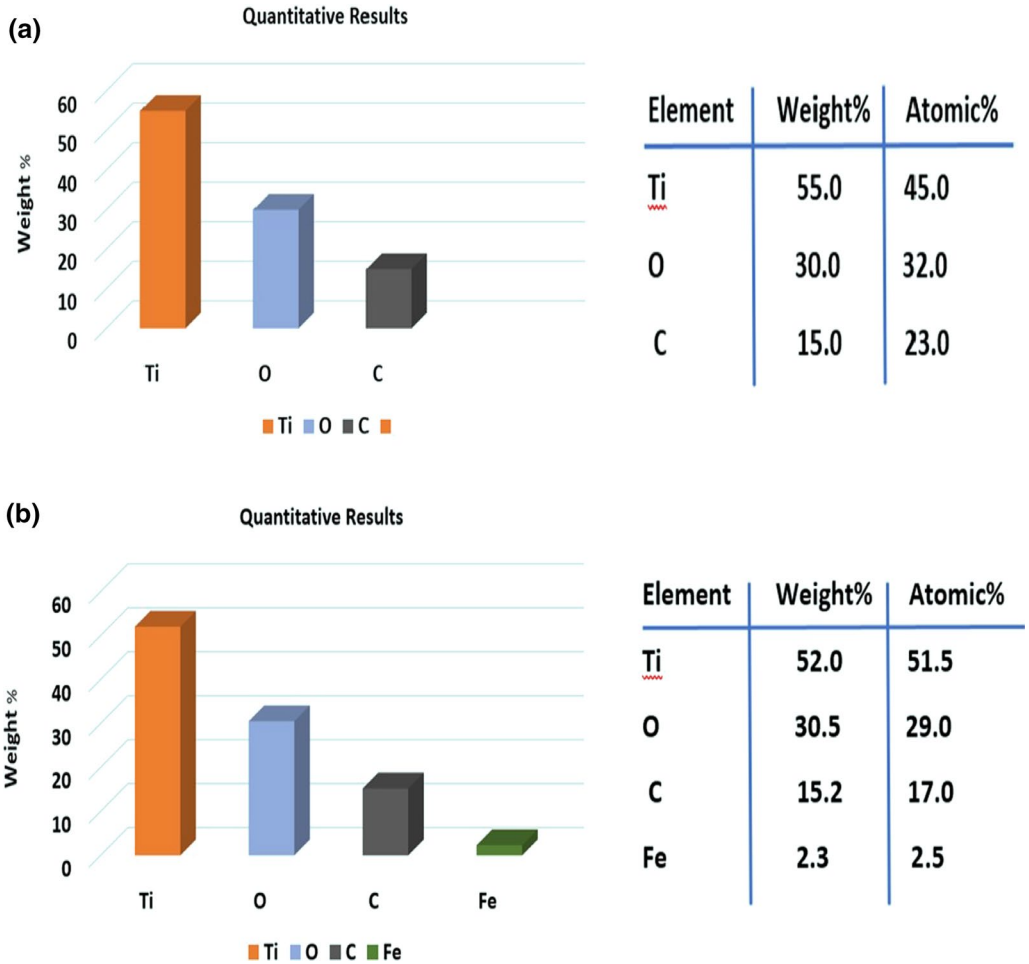

Element	Weight%	Atomic%
Ti	55.0	45.0
O	30.0	32.0
C	15.0	23.0

Element	Weight%	Atomic%
Ti	52.0	51.5
O	30.5	29.0
C	15.2	17.0
Fe	2.3	2.5

Fig. 3 (a) EDX of un-doped TiO_2 with respective atomic weight percentages. (b) EDX of Fe:TiO_2 with respective atomic weight percentages.

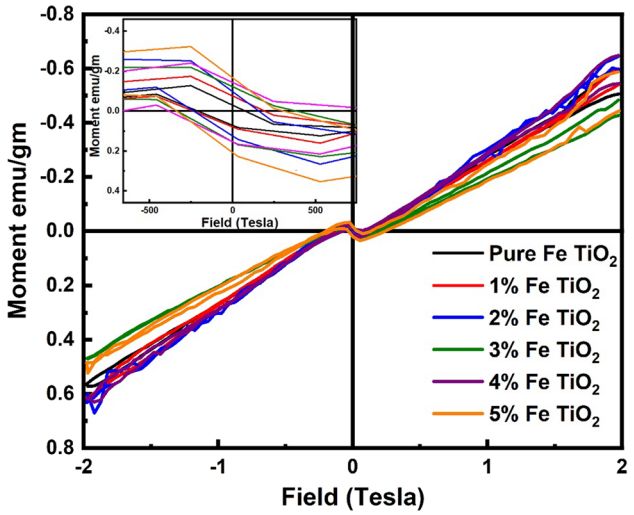

Fig. 4 M–H curve of un-doped TiO_2 and Fe:TiO_2 samples.

Table I Different parameters like magnetization (M_s), retentivity (M_r), coercivity (H_c) calculated from the hysteresis loop

α-Fe_2O_3:TiO_2			
wt.%	Saturation magnetization (M_s)—emu/gm	Coercivity (M_c)—Gauss	Retentivity (M_r)—emu/gm
0	0.55	141.74	3.33
1	0.57	212.61	5.35
2	0.62	191.35	2.05
3	0.25	361.45	2.52
4	0.59	559.88	2.72
5	0.22	318.92	3.43

However, four factors are responsible for magnetization: (i) O_2 vacancy, (ii) magnetic metal (unpaired *d* electrons), (iii) point defects, and (iv) the oxidation state of titanium (Ti^{3+}).[18] Another important parameter is an alteration in electrons in *s*, *p*, and *d* orbitals with the addition of transition metal in TiO_2.

Room-temperature magnetic studies were done for all the Fe_2O_3-doped TiO_2 powder samples at 2 tesla. The shape of M–H loops agrees with the paramagnetic behavior. The magnetic retentivity (M_r), coercive field (H_c), and magnetization (M_s) were calculated, as shown in the inset of the hysteresis loop in Fig. 4, and calculated values are presented in Table I. Slight diamagnetic behavior is also observed at low magnetic fields that may be due to low magnetic doping and dominant TiO_2 content (see inset of Fig. 4).

Figure 5a shows the rise of spontaneous magnetization with Fe doping percentage in TiO_2 and Fig. 5b shows the growth of saturation magnetization in the 2% Fe:TiO_2 sample with the doping percentage of Fe in TiO_2. Generally, it is observed that with the rise in dopant levels, magnetization improves; however, here, an inverse order is observed: with a rise in Fe content, a decline in magnetization is observed. Maximum magnetization of 6.2×10^{-1} emu/gm is exhibited by the 2% Fe:TiO_2. Similar results were shown by Waseem. Annealing of samples also gives rise to oxygen vacancies, a major cause of magnetism, as observed by Khaibullin.[19]

Optical Study UV–Vis, and PL

The absorption spectrum and bandgap (E_g) of Fe_2O_3-doped TiO_2 samples were studied using UV–Vis analysis, as shown in Fig. 6. The Fe:TiO_2 showed a rise in absorption and showed a redshift to un-doped TiO_2.The precise value

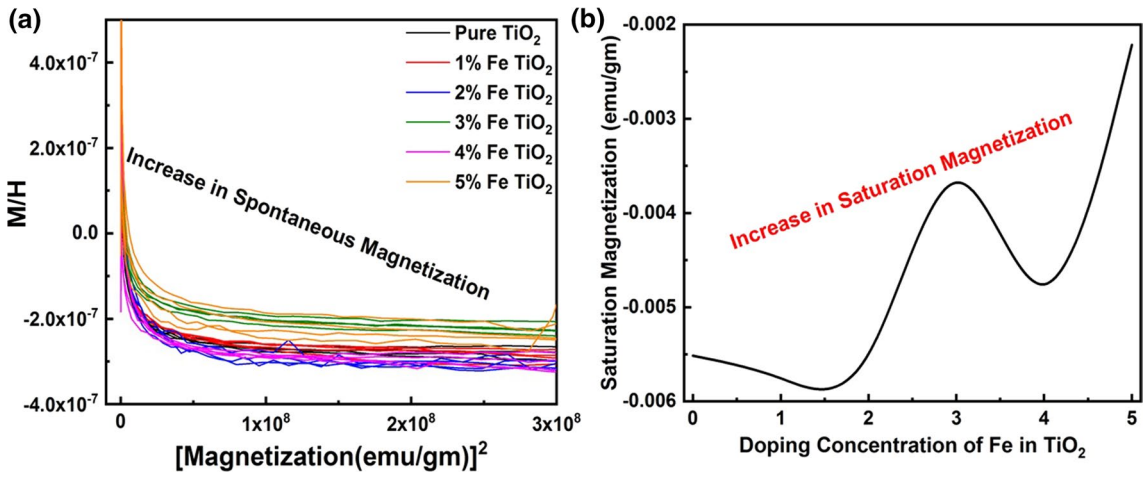

Fig. 5 (a) Spontaneous magnetization with the doping percentage of Fe in TiO_2. (b) Saturation magnetization with the doping percentage of Fe in TiO_2.

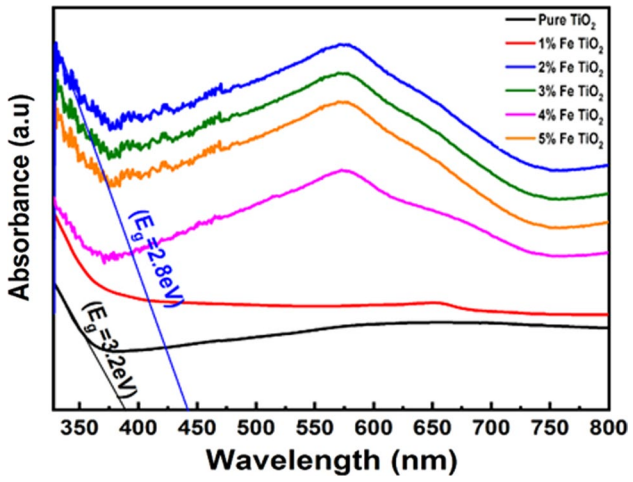

Fig. 6 UV spectra of un-doped TiO_2 and Fe:TiO_2 samples.

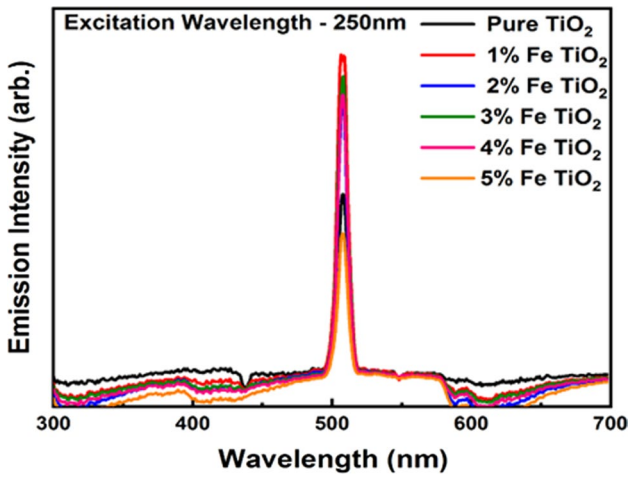

Fig. 7 PL spectra of un-doped TiO_2 and Fe:TiO_2 samples.

of E_g for TiO_2 was calculated indirectly using the intercept of the tangent-slope method. According to previous reports, narrowing of the bandgap of TiO_2 by iron doping can be due to two factors: (1) a charge transfer transition between TiO_2 and (2) a transition of *d* electrons to the valence or conduction band or *d*–*d* transition among the Fe atoms.[7] The bandgap value for Fe:TiO_2 (3.15 eV) decreases from TiO_2 ($E_g = 3.26$ eV). The thin bandgap and redshift of the Fe:TiO_2 spectra indicate that Fe:TiO_2 absorbed light with a wider wavelength range (≤ 394 nm), whereas the result for TiO_2 was ≤ 380 nm. Therefore, the Fe^{2+}/Fe^{3+} ions in Fe:TiO_2 contribute to a large number of dopant levels. Thus, the redshift in wavelength is observed with the addition of (Fe^{2+}/Fe^{3+}) in TiO_2.[20,21]

Luminescence spectra of all the Fe_2O_3-doped TiO_2 samples are presented in Fig. 7. The PL emission results in a sequence of recombination centers of charge carriers with the increase in doping, consequently increasing the radiative recombination of electron–hole pairs in TiO_2. There is an enhanced PL spectral intensity with doping in TiO_2 up to 2%, and then it deteriorates subsequently; the electron–hole recombination increases with more Fe in TiO_2.[22] When the recombination increases, the lower number of charge carriers prevents mobility with the increasing iron percentages; thus, luminescence decreases up to 2% Fe:TiO_2.

With the rise in Fe percentage above 2% in Fe:TiO_2, PL intensities corresponding to Fe^{3+} increase remarkably; this further promotes the addition of electron-trapped agents in TiO_2, resulting in electron–hole separation. This clarifies that Fe fits well into the TiO_2 with low doping percentages, whereas excess Fe^{3+} agglomerates.[23]

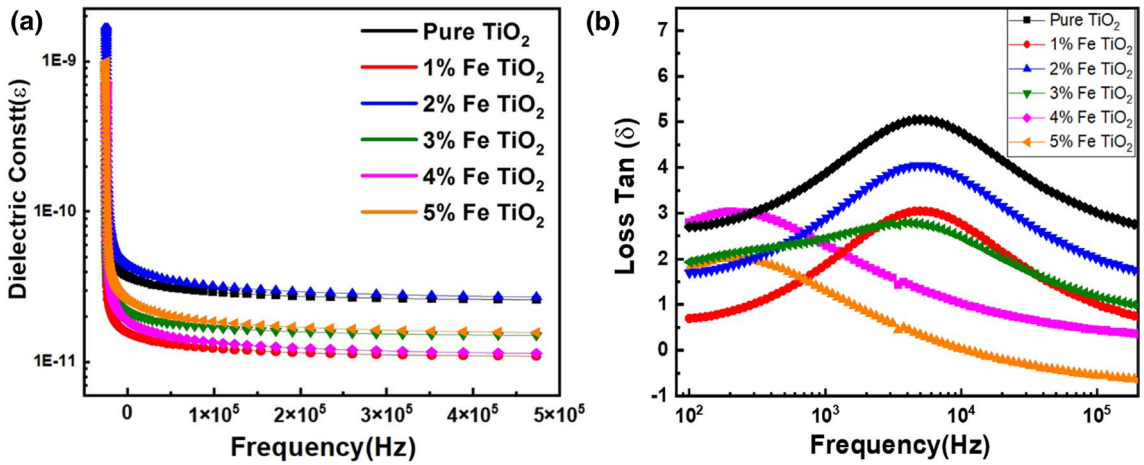

Fig. 8 (a) Dielectric constant versus frequency (Hz) of un-doped TiO_2 and Fe:TiO_2 samples. (b) Dielectric loss versus frequency (Hz) of un-doped TiO_2 and Fe:TiO_2 samples.

Electrical Study

Room-temperature dielectric studies were performed for all Fe_2O_3-doped TiO_2 samples, shown in Fig. 8a and b. The dielectric behavior of the 2% Fe:TiO_2 sample showed a high dielectric constant value because more charge carriers participate compared to the un-doped and heavily doped samples.[24] Un-doped TiO_2 and low-Fe TiO_2 have maximum –OH adsorption on the plane because of high charge concentration. As per earlier reports, anatase TiO_2 is hydrophilic, where –OH groups are present on the surface; as the size of the particles decreases, the area/unit volume rises, in comparison with the concentration of –OH, present in a unit volume, which reaches a higher value. As evident by XRD, the crystallite size decreases with the addition of Fe content above 2%. The appearance of the metastable anatase phase also explains the strange dielectric behavior of other samples in a small frequency range.[25–27]

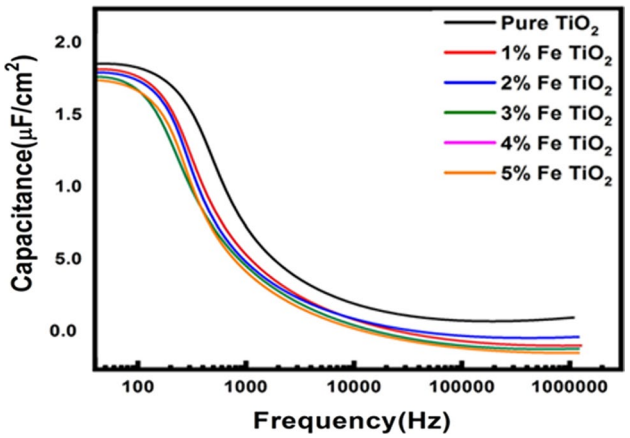

Fig. 9 Capacitance versus frequency of all un-doped TiO_2 and Fe:TiO_2 samples.

Figure 9 depicts the capacitance versus frequency (Hz) curve of all Fe_2O_3-doped TiO_2 samples. Decreases in capacitance with an increase in the size of the particle is in accordance with doping percentage from un-doped TiO_2 to the 5% Fe TiO_2. Similarly, XRD confirms the formation of additional phases with higher doping percentages of Fe in TiO_2. Correspondingly, PL results also support the same as the doping percentage of Fe increases, which promotes a number of mobility defect states.[28] As per the author's knowledge, we have achieved a maximum magnetization of 0.62 emu/gm for the lowest Fe percentage of 2% in TiO_2; moreover, the synthesis duration is nearly 2 h, which is also unique as compared to other reported research, which took hours to days. Table II shows that we have studied the detailed magnetic, optical, and electrical properties of all samples to confirm the best doping percentage of Fe is 2% in TiO_2.[8,9,11,24,25,29–50]

Conclusions

All un-doped TiO_2 and (1–5 wt.%) Fe:TiO_2 powders were synthesized by high-temperature solid-state reaction, and the results correlated well with the magnetic, optical, and electrical studies in Fe:TiO_2. All the studies mainly revealed that 2% Fe:TiO_2 seems to be an optimized material exhibiting superior properties. XRD confirms that 2% Fe does not affect the basic structure of un-doped TiO_2. The presence of a secondary phase with an increase in Fe doping percentage above 2% Fe was observed. Magnetically, all Fe:TiO_2 samples are paramagnetic, whereas 2% Fe:TiO_2 has maximum magnetization. The PL spectra

Table II Comparison of magnetic, optical, and electrical properties of previous research

S. No. references	Before 2005[25, 29–34]	2005–2010[11, 35–41]	2010–2015[24, 42–47]	2015–2017[48, 49]	2017–2020[8, 9, 50]	Our research
Synthesis route	Hydrothermal, mechanical alloying, etc.	Liquid-phase deposition, sol–gel, etc.	RF sputtering thermal plasma, etc.	Flame spray, pyrolysis, etc.	Atomic layer deposition, etc.	Solid-state reaction
Synthesis time	≥ 24 h	≥ 50 h	≥ 5 h	≥ 20 h	≥ 2 h	2h
Conc^n of Fe in TiO_2	Low Fe conc^n	0.1–0.3 mol and at higher conc^n (0–15 wt.%)	0.2, 0.5, 0.8, 0.17, and 0.28	Low Fe Conc^n toxicity tests	0.1, 4, 6, 10%	0–5% Fe
Maximum magnetization	0.5 emu/gm for 3%	$(2.12–1.51)\times10^{-2}$ emu/gm	–	–	Rise in paramagnetism with Fe Conc^n	Paramagnetic 0.62 emu/gm for 2% Fe Conc^n
Optical studies	Photocatalysis studies with dye	Photocatalysis studies with dye	Redshift absorption edge	Bandgap shift to the lower edge	–	Redshift with Fe Conc^n
Electrical studies	10^{-6} s/m	–	–	–	~0.1–0.6 V/cm^2	~1.8 (μF/cm^2)

of un-doped TiO_2 and Fe:TiO_2 samples showed sharp emission. SEM pictures have proven that all the particle agglomerates are within 50 nm. From the above investigations, 2% Fe in TiO_2 may be considered the optimized ratio for effective magneto-opto-electro device applications.

Acknowledgments The authors would like to acknowledge the Director of the Council of Scientific & Industrial Research National Physical Laboratory (CSIR-NPL) India for supporting the research work and providing the necessary characterization facilities. The author Divya Rehani sincerely acknowledges the Council of Scientific & Industrial Research (CSIR) for providing a Senior Research Fellowship (#31/1(0569)/2019-EMR-1.

Conflict of interest The authors declare no conflicts of interest.

References

1. J. Wang, R. Limas-Ballesteros, T. Lopez, A. Moreno, R. Gomez, O. Novaro, and X. Bokhimi, Quantitative determination of titanium lattice defects and solid-state reaction mechanism in iron-doped TiO_2 photocatalysts. *J. Phys. Chem. B* 105(40), 9692–9698 (2001).
2. I. Ganesh, P.P. Kumar, A.K. Gupta, P.S. Sekhar, K. Radha, G. Padmanabham, and G. Sundararajan, Preparation and characterization of Fe-doped TiO_2 powders for solar light response and photocatalytic applications. *Process. Appl. Ceram.* 6(1), 21–36 (2012).
3. D. Rehani, S. Bishnoi, M. Saxena, and S.N. Sharma, Magneto-opto electronic applications of conductive and room temperature ferromagnetic (Al, Mn) Co-doped ZnO particles with visible emission. *J. Nanosci. Nanotechnol.* 20(6), 3913–3918 (2020).
4. D. Rehani, S. Bishnoi, M. Saxena, D. Haranath, V. Gupta, and S.N. Sharma, Efficient luminomagnetic and conductive Eu and Dy doped ZnO phosphors for multifunctional devices. *J. Phys. Chem. Solids* 143, 109460 (2020).
5. W.-Q. Han, W. Wen, D. Yi, Z. Liu, M.M. Maye, L. Lewis, J. Hanson, and O. Gang, Fe-doped trititanate nanotubes: formation, optical and magnetic properties, and catalytic applications. *J. Phys. Chem. C* 111(39), 14339–14342 (2007).
6. X. Sun and Y. Li, Synthesis and characterization of ion-exchangeable titanate nanotubes. *Chem. A Eur. J.* 9(10), 2229–2238 (2003).
7. D. Wu, Y. Chen, J. Liu, X. Zhao, A. Li, and N. Ming, Co-doped titanate nanotubes. *Appl. Phys. Lett.* 87(11), 112501 (2005).
8. H. Rasoulnezhad, G. Hosseinzadeh, N. Ghasemian, R. Hosseinzadeh, and A.H. Keihan, Transparent nanostructured Fe-doped TiO_2 thin films prepared by ultrasonic assisted spray pyrolysis technique. *Mater. Res. Express* 5(5), 056401 (2018).
9. Z.N.N. Kayani, I. Wahid, Z. Saddiqe, S. Riaz, S. Waseem, and S. Naseem, Tailoring of optical, biological and magnetic properties of nanocrystalline Fe doped TiO_2 thin films. *Mater. Res. Express* 6(12), 1250h2 (2020).
10. M. Crişan, M. Răileanu, N. Drăgan, D. Crişan, A. Ianculescu, I. Niţoi, P. Oancea, S. Şomăcescu, N. Stănică, and B. Vasile, Sol–gel iron-doped TiO_2 nanopowders with photocatalytic activity. *Appl. Catal. A* 504, 130–142 (2015).
11. X. Wang, J.-G. Li, H. Kamiyama, M. Katada, N. Ohashi, Y. Moriyoshi, and T. Ishigaki, Pyrogenic iron (III)-doped TiO_2 nanopowders synthesized in RF thermal plasma: phase formation, defect structure, band gap, and magnetic properties. *J. Am. Chem. Soc.* 127(31), 10982–10990 (2005).
12. M. Yeganeh, N. Shahtahmasebi, A. Kompany, M. Karimipour, F. Razavi, N. Nasralla, and L. Šiller, The magnetic characterization of Fe doped TiO_2 semiconducting oxide nanoparticles synthesized by sol–gel method. *Physica B* 511, 89–98 (2017).
13. D. Rehani, S. Bishnoi, M. Saxena, and S.N. Sharma, Optimized Fe-doped ZnO nanoparticles for magneto-opto device applications. *Mater. Today Proc.* 32, 417–421 (2020).
14. G. Viruthagiri, P. Praveen, N. Shanmugam, and S. Mugundan, Preparation, structural and optical characterization of fe doped TiO_2 nanoparticles (2013).
15. B. Santara, P. Giri, S. Dhara, K. Imakita, and M. Fujii, Oxygen vacancy-mediated enhanced ferromagnetism in undoped and Fe-doped TiO_2 nanoribbons. *J. Phys. D Appl. Phys.* 47(23), 235304 (2014).
16. C. Rodriguez-Torres, A. Cabrera, L. Errico, C. Adan, F. Requejo, M. Weissmann, and S. Stewart, Local structure and magnetic behaviour of Fe-doped TiO_2 anatase nanoparticles: experiments and calculations. *J. Phys. Condens. Matter* 20(13), 135210 (2008).
17. K. Bapna, D. Phase, and R. Choudhary, Study of valence band structure of Fe doped anatase TiO_2 thin films. *J. Appl. Phys.* 110(4), 043910 (2011).
18. S. Waseem, S. Anjum, L. Mustafa, T. Zeeshan, Z.N. Kayani, and K. Javed, Structural, magnetic and optical investigations of Fe and Ni co-doped TiO_2 dilute magnetic semiconductors. *Ceram. Int.* 44(15), 17767–17774 (2018).
19. R. Khaibullin, L. Tagirov, B. Rameev, S.Z. Ibragimov, F. Yildiz, and B. Aktaş, High curie-temperature ferromagnetism in cobalt-implanted single-crystalline rutile. *J. Phys. Condens. Matter* 16(41), L443 (2004).
20. C. Xu, Y. Zhang, J. Chen, J. Lin, X. Zhang, Z. Wang, and J. Zhou, Enhanced mechanism of the photo-thermochemical cycle based on effective Fe-doping TiO_2 films and DFT calculations. *Appl. Catal. B* 204, 324–334 (2017).
21. D. Zhang, Enhanced photocatalytic activity for titanium dioxide by co-modification with copper and iron. *Transit. Met. Chem.* 35(8), 933–938 (2010).
22. S. Delekar, H. Yadav, S. Achary, S. Meena, and S. Pawar, Structural refinement and photocatalytic activity of Fe-doped anatase TiO_2 nanoparticles. *Appl. Surf. Sci.* 263, 536–545 (2012).
23. O. Carp, C.L. Huisman, and A. Reller, Photoinduced reactivity of titanium dioxide. *Prog. Solid State Chem.* 32(1–2), 33–177 (2004).
24. D. Singh, P. Yadav, N. Singh, C. Kant, M. Kumar, S.D. Sharma, and K. Saini, Dielectric properties of Fe-doped TiO_2 nanoparticles synthesised by sol–gel route. *J. Exp. Nanosci.* 8(2), 171–183 (2013).
25. A. Bally, E. Korobeinikova, P. Schmid, F. Levy, and F. Bussy, Structural and electrical properties of Fe-doped thin films. *J. Phys. D Appl. Phys.* 31(10), 1149 (1998).
26. A. Kumar, M.K. Kashyap, N. Sabharwal, S. Kumar, A. Kumar, P. Kumar, and K. Asokan, Impedance analysis and dielectric response of anatase TiO_2 nanoparticles codoped with Mn and Co ions. *Mater Res. Express* 4(11), 115035 (2017).
27. A. Wypych, I. Bobowska, M. Tracz, A. Opasinska, S. Kadlubowski, A. Krzywania-Kaliszewska, J. Grobelny, and P. Wojciechowski, Dielectric properties and characterisation of titanium dioxide obtained by different chemistry methods. *J. Nanomater.* (2014). https://doi.org/10.1155/2014/124814.
28. T. Nabatame, A. Ohi, T. Chikyo, M. Kimura, H. Yamada, and T. Ohishi, Electrical properties of anatase TiO_2 films by atomic layer deposition and low annealing temperature. *J. Vac. Sci. Technol. B Nanotechnol. Microelectron. Mater. Process. Meas. Phenom.* 32(3), 03D121 (2014).
29. Y. Wang, H. Cheng, Y. Hao, J. Ma, W. Li, and S.J.J. Cai, Preparation, characterization and photoelectrochemical behaviors of Fe

(III)-doped TiO_2 nanoparticles. *J. Mater. Sci.* 34(15), 3721–3729 (1999).
30. Y.-H. Zhang and A.J.J. Reller, Nanocrystalline iron-doped mesoporous titania and its phase transition. *J. Mater. Chem.* 11(10), 2537–2541 (2001).
31. R. Sonawane, B. Kale, and M.J.M.C. Dongare, Physics, preparation and photo-catalytic activity of Fe–TiO_2 thin films prepared by sol–gel dip coating. *Mater. Chem. Phys.* 85(1), 52–57 (2004).
32. J. Zhu, W. Zheng, B. He, J. Zhang, and M.J.J. Anpo, Characterization of Fe–TiO_2 photocatalysts synthesized by hydrothermal method and their photocatalytic reactivity for photodegradation of XRG dye diluted in water. *J. Mole. Catal. A Chem.* 216(1), 35–43 (2004).
33. D.H. Kim, H.S. Hong, S.J. Kim, J.S. Song, and K.S.J. Lee, Compounds, Photocatalytic behaviors and structural characterization of nanocrystalline Fe-doped TiO_2 synthesized by mechanical alloying. *J. Alloys Compd.* 375(1–2), 259–264 (2004).
34. N.H. Hong, J. Sakai, and W.J.J. Prellier, Distribution of dopant in Fe: TiO_2 and Ni: TiO_2 thin films. *J. Magn. Magn. Mater.* 281(2–3), 347–352 (2004).
35. M. Zhou, J. Yu, and B.J.J. Cheng, Effects of Fe-doping on the photocatalytic activity of mesoporous TiO_2 powders prepared by an ultrasonic method. *J. Hazard. Mater.* 137(3), 1838–1847 (2006).
36. J. Yu, H. Yu, C. Ao, S. Lee, C.Y. Jimmy, and W. Ho, Preparation, characterization and photocatalytic activity of in situ Fe-doped TiO_2 thin films. *Thin Solid Films* 496(2), 273–280 (2006).
37. J. Zhu, J. Ren, Y. Huo, Z. Bian, and H. Li, Nanocrystalline Fe/TiO_2 visible photocatalyst with a mesoporous structure prepared via a nonhydrolytic sol–gel route. *J. Phys. Chem. C* 111(51), 18965–18969 (2007).
38. W.Y. Teoh, R. Amal, L. Mädler, and S.E. Pratsinis, Flame sprayed visible light-active Fe-TiO_2 for photomineralisation of oxalic acid. *Catal. Today* 120(2), 203–213 (2007).
39. M. Cernea, C. Valsangiacom, R. Trusca, and F. Vasiliu, Synthesis of iron-doped anatase-TiO_2 powders by a particulate sol–gel route. *J. Optoelectron. Adv. Mater.* 9(8), 2648–2652 (2007).
40. W.-C. Hung, Y.-C. Chen, H. Chu, and T.K. Tseng, Synthesis and characterization of TiO_2 and Fe/TiO_2 nanoparticles and their performance for photocatalytic degradation of 1,2-dichloroethane. *Appl. Surf. Sci.* 255(5), 2205–2213 (2008).
41. Z. Ambrus, N. Balázs, T. Alapi, G. Wittmann, P. Sipos, A. Dombi, and K. Mogyorósi, Synthesis, structure and photocatalytic properties of Fe(III)-doped TiO_2 prepared from $TiCl_3$. *Appl. Catal. B Environ.* 81(1–2), 27–37 (2008).
42. C.L. Luu, Q.T. Nguyen, and S.T. Ho, Synthesis and characterization of Fe-doped TiO_2 photocatalyst by the sol–gel method. *Adv. Nat. Sci. Nanosci. Nanotechnol.* 1(1), 015008 (2010).
43. S. George, S. Pokhrel, Z. Ji, B.L. Henderson, T. Xia, L. Li, J.I. Zink, A.E. Nel, and L.J. Mädler, Role of Fe doping in tuning the band gap of TiO_2 for the photo-oxidation-induced cytotoxicity paradigm. *J. Am. Chem. Soc.* 133(29), 11270–11278 (2011).
44. R.D.S. Santos, G.A. Faria, C. Giles, C.A. Leite, H.D.S. Barbosa, M.A. Arruda, and C. Longo, Iron insertion and hematite segregation on Fe-doped TiO_2 nanoparticles obtained from sol–gel and hydrothermal methods. *ACS Appl. Mater. Interfaces* 4(10), 5555–5561 (2012).
45. J.-W. Ok, H.-D. Park, and Y.-M. Sung, Growth and properties of Ti films formed by dc magnetron sputtering for TCO-free photo electrode applications. *Electron. Mater. Lett.* 9, 527–530 (2013).
46. N. Nasralla, M. Yeganeh, Y. Astuti, S. Piticharoenphun, N. Shahtahmasebi, A. Kompany, M. Karimipour, B.G. Mendis, N.R.J. Poolton, and L. Šiller, Structural and spectroscopic study of Fe-doped TiO_2 nanoparticles prepared by sol–gel method. *Sci. Iran.* 20(3), 1018–1022 (2013).
47. T. Nabatame, A. Ohi, T. Chikyo, M. Kimura, H. Yamada, and T. Ohishi, Electrical properties of anatase TiO_2 films by atomic layer deposition and low annealing temperature. *J. Vac. Sci. Technol. B, Nanotechnol. Microelectron. Mater. Process. Meas. Phenom.* 32(3), 03D121 (2014).
48. Y. Liu, J.-F. Wan, C.-T. Liu, and Y.-B. Li, Fabrication of magnetic Fe_3O_4/C/TiO_2 composites with nanotube structure and enhanced photocatalytic activity. *Mater. Sci. Technol.* 32, 786–793 (2016).
49. H. Choi, H. Ryu, and W.-J. Lee, Study of the morphological, optical, structural and photoelectrochemical properties of TiO_2 nanorods grown with various precursor concentrations. *Electron. Mater. Lett.* 13, 497–504 (2017).
50. R. Zahid, M. Manzoor, A. Rafiq, M. Ikram, M. Nafees, A.R. Butt, S.G. Hussain, and S. Ali, Influence of iron doping on structural, optical and magnetic properties of TiO_2 nanoparticles. *Electron. Mater. Lett.* 14, 587–593 (2018).

Authors and Affiliations

Divya Rehani[1,2] · Manish Saxena[3] · Sanjay R. Dhakate[2] · Shailesh Narain Sharma[2]

[1] Dr. A.P.J. Abdul Kalam Technical University, Lucknow, Uttar Pradesh 226031, India

[2] CSIR- National Physical Laboratory, Dr. K.S. Krishnan Marg, New Delhi 110012, India

[3] Moradabad Institute of Technology, Moradabad, U.P 244001, India